ISBN: 978-3-95450-179-3 doi:10.18429/JACoW-FEL2017-TUB01

SEEDING EXPERIMENTS AND SEEDING OPTIONS FOR LCLS II

E. Hemsing†, R. Coffee, G. Dakovski, W. Fawley, Y. Feng, B. Garcia, J. Hastings,
Z. Huang, G. Marcus, D. Ratner, T. Raubenheimer, and R. W. Schoenlein
SLAC National Accelerator Laboratory
G. Penn
Lawrence Berkeley National Accelerator Laboratory

Abstract

We discuss the present status of FEL seeding experiments toward the soft x-ray regime and on-going studies on possible seeding options for the high repetition soft x-ray line at LCLS-II. The seeding schemes include self-seeding, cascaded HGHG, EEHG, and possible hybrid methods to reach the 1-2 nm regime with the highest possible brightness and minimal spectral pedestal. We describe relevant figures of merit, performance expectations, and potential issues.

INTRODUCTION

The general motivation for FEL seeding arises from the need for control over the longitudinal coherence. At soft x-rays, the ability to trade-off time-resolution (10-60 fs) and spectral resolution (180-30 meV) at close to the Fourier transform limit will open new dimensions in X-ray science.

Many seeding methods have been proposed to produce transform limited pulses down to soft x-rays. The three leading candidates are soft x-ray self seeding (SXRSS), Cascaded high gain harmonic generation (HGHG), and Echo Enabled Harmonic Generation (EEHG). SXRSS uses the monochromatized output from an upstream section of the FEL to seed the downstream section to saturation. It is currently the most mature technology in the 1-2 nm regime, as it has been demonstrated and delivered to users at LCLS for several years [1]. Cascaded HGHG uses external lasers to generate harmonic bunching and is in regular use at the FERMI FEL at Sincrotrone Trieste on the FEL-2 line where it is used to reach the 4-nm water window with peak fluences of order 10 μJ [2]. FERMI is currently operating as a user facility and has proved to be attractive for experiments that require wavelength tunability, multicolor pulses, polarization tunability, and higher coherence than is generally available from SASE-based FELs. EEHG also uses external lasers [3–8] and has been experimentally tested at wavelengths down to 32 nm [9], but has yet to demonstrated at soft x-rays, though efforts are underway [10, 11].

We have recently conducted studies on seeding for the high repetition soft x-ray line at LCLS-II. We find that the most promising candidates at this stage are SXRSS and EEHG as judged by anticipated performance, sensitivity, and flexibility, though there are clear challenges with both schemes. We show and compare their expected performance both in the case of ideal beams and more realistic start-to-end (S2E) beams. Other seeding methods like cascaded HGHG or even direct high harmonic generation (HHG) seeding are not among the most promising candidates at this stage due to anticipated poor performance or lack of current technical maturity. For example, we find through detailed simulations that cascaded HGHG is highly sensitive to the electron beam phase space distribution and that the spectral quality is comparable to SASE at the 1-2 nm level. The HHG technique is even more limited in its ability to access the required performance criteria due to poor ($\lesssim 10^{-6}$) harmonic conversion efficiency at shorter wavelengths. Upcoming proof-of-principle experiments on hybrid schemes like cascaded EEHG or EEHG/HGHG combinations, or on alternate techniques like coherent inverse Compton scattering may provide key information on their use as potential options, but currently these concepts are only in the preliminary experimental stages.

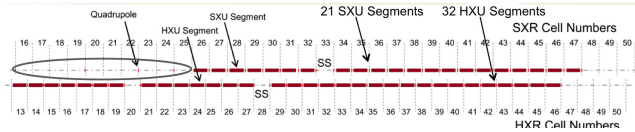

Figure 1: Layout of LCLS-II soft x-ray (top) and hard x-ray (bottom) undulators.

PERFORMANCE GOALS

The expectation for any seeding scheme in LCLS-II is the production of temporally coherent pulses with sufficient spectral brightness to address the photon science requirements. These requirements include several features that favor a seeded FEL with many characteristics inherent to optical laser systems:

- Enhanced Control: Precision control of the central wavelength well within the SASE bandwidth, as well as the ability to control the coherent bandwidth.
- Minimal Spectral Pedestal: The microbunching instability (MBI) is predicted to be a significant effect at the LCLS-II. It is believed to be responsible for the limited resolving power (roughly 2000-5000) of the SXRSS at LCLS [1, 12, 13]. Recent studies indicate that EEHG has a reduced sensitivity to MBI under certain conditions [14].
- Coherent Two/Multi Color Operations: Several different schemes to produce two-color x-ray pulses with variable pulse energy separations and timing delay have

† ehemsing@slac.stanford.edu

ISBN: 978-3-95450-179-3 doi:10.18429/JACoW-FEL2017-TUB01

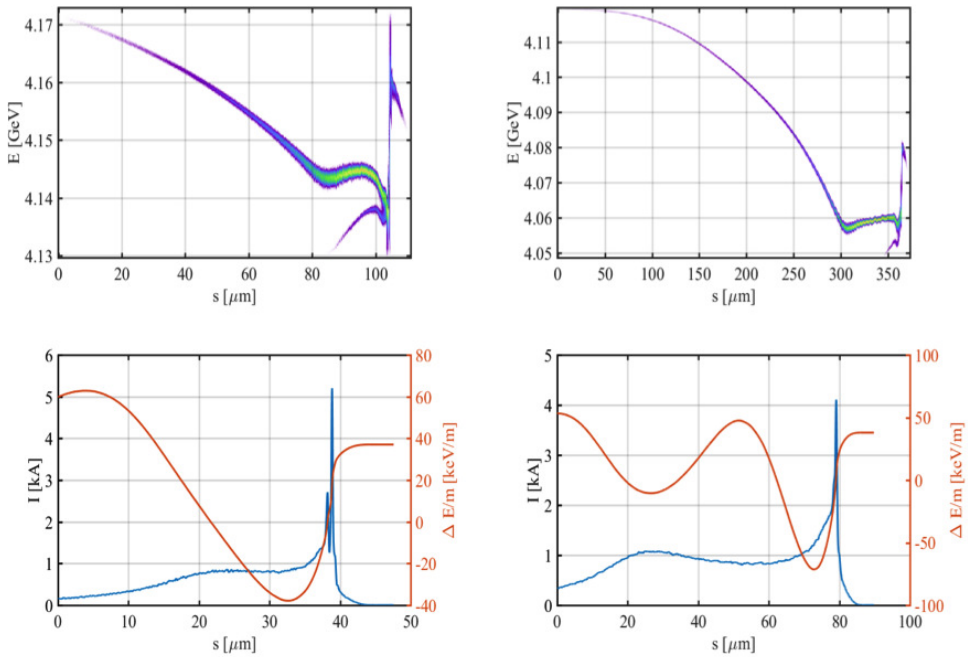

Figure 2: 100 pC and 300 pC electron beams from start-to-undulator IMPACT optimizations used for LCLS-II FEL simulations (head is to the right of the figures). Top left: Longitudinal phase space of 100 pC electron beam. Bottom Left: Current profile of the head and core of the 100 pC electron beam as well as the time-dependent energy loss per meter of distance in the undulator due to resistive wall wakefields. Top Right: Longitudinal phase space of 300 pC electron beam. Bottom Right: Current profile of the head and core of the 300 pC electron beam as well as the time-dependent energy loss per meter of distance in the undulator due to resistive wall wakefields.

recently been demonstrated at LCLS [15–17]. Multiple colors can be seeded at hard x-rays with the crystal monochromator, but such techniques do not translate to the SXRSS grating monochromator. Multicolor pulses have been produced at the FERMI FEL via the single stage HGHG configuration [18], and similar such methods could be extended to soft x-rays with EEHG.

LCLS-II LAYOUT

The layout of the LCLS-II undulators is shown in Figure 1. There is ~40 m of space available upstream of the soft x-ray line (circled) that could be used for external seeding infrastructure. Each of the 21 soft x-ray undulator segments have a λ_u=39 mm period and are variable gap. The total length is 96 m, with each segment is 3.4 m long and and separated by a 1 m break. LCLS-II electron beam parameters are listed in Table 1.

QUANTIFYING PERFORMANCE

The measures of performance that aid in comparing different schemes are the peak photon density (photons/meV), the "FWHM-equivalent" bandwidth, ΔE_e, and the dimensionless brightness B_e. The ΔE_e is useful in capturing the contribution of the pedestal and is defined by the minimum spectral extent that contains 76% of the total pulse energy E. This corresponds to the fraction that a 1-D Gaussian contains in the FWHM central region. From this we can define a dimensionless brightness $B_e = 0.76 * E/\Delta E_e$, which is the number of photons contained within the FWHM-equivalent bandwidth.

START-TO-END BEAMS

The IMPACT code was used to track both a 100 pC and a 300 pC electron beam (two standard configurations as of early 2017) from the cathode to the LCLS-II SXR undulator. The upper panels of Fig. 2 show the predicted longitudinal phase space of each beam. Note the apparent energy oscillations developed from MBI growth, the curvature in the beam core, and the long tails. We stress that these

Table 1: LCLS-II SXR Electron Beam Parameters

Parameter	Value
Energy	4 GeV
Charge	100-300 pC
Peak Current	1 kA
Emittance	0.45 mm-mrad
Energy Spread	500 keV
Beta Function	12 m

ISBN: 978-3-95450-179-3 doi:10.18429/JACoW-FEL2017-TUB01

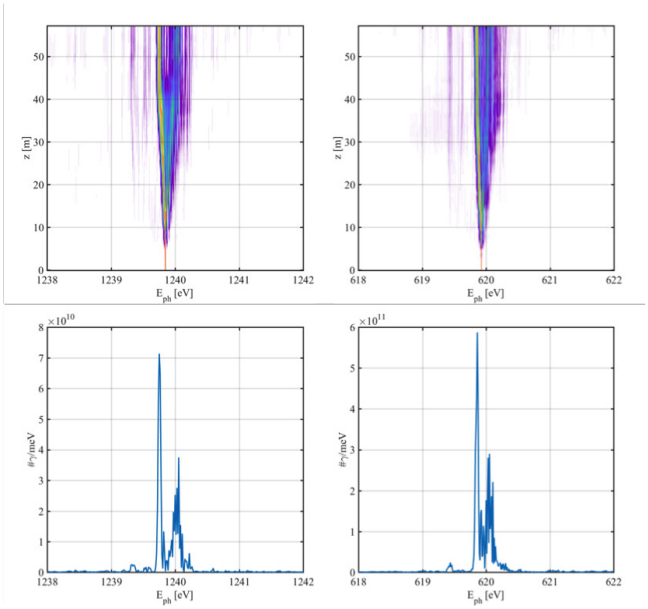

Figure 3: 300 pC beam SXRSS simulation results at 1 nm (left) and 2 nm (right).

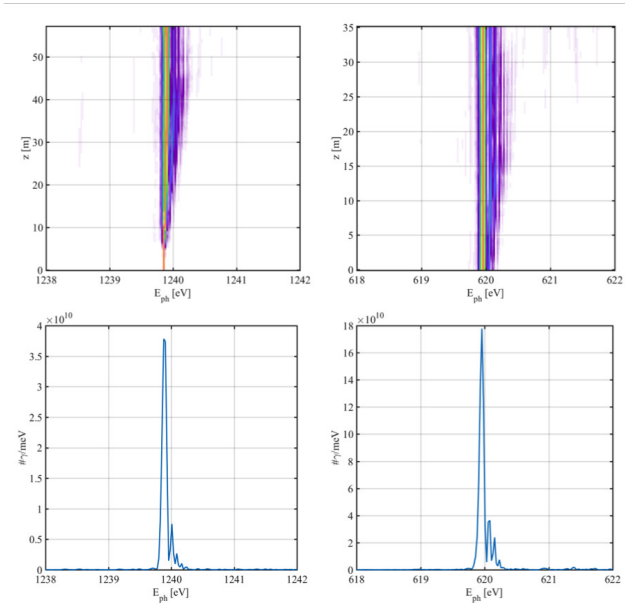

Figure 4: 100 pC beam SXRSS simulation results at 1 nm (left) and 2 nm (right).

beams are optimized primarily for low transverse emittance and high current, and are thus not necessarily optimized for seeding. Beams that are optimized better for seeding are currently under study. Figure 2 also shows the current profile of the head and core of each electron beam as well as the predicted time-dependent electron energy loss (in keV) per meter of distance travelled in the undulator due to the resistive wall wakefield. These long wavelength energy modulations broaden the bandwidth of a seeded FEL spectrum even in the absence of MBI-driven energy or density modulations.

SXRSS S2E

Figure 3 shows the spectra and normalized spectral evolution of the 1 and 2 nm cases with the 300 pC beam. An ideal seed is assumed from the SXRSS monochrometer. In both cases, the spectrum has a clear bifurcation around z = 30 m (measured from the SXRSS section) due primarily to the long wavelength energy modulation imprinted on the electron beam from the resistive wall wakefield. The lower panels of Figure 3 show the spectra at the peak of the spectral brightness, which is at the end of the undulator. Clear spectral splitting is evident from the two dominant peaks, the largest of which has a FWHM of 55 meV. However, the splitting leads to a ΔE_e=600 meV at 1 nm and ΔE_e=400 meV at 2 nm. Less prominent but still evident are the effects of MBI-induced energy modulations, which drive the amplification of pedestal photon energies.

Figure 4 shows the spectra for the 100 pC LCLS-II beam. The performance is much better than the 300 pC case, due primarily to the shorter bunch length (20μm compared to 80μm) which is not as susceptible to resistive wall wakefield-driven bandwidth splitting. While MBI-driven modulations still serve to amplify frequency content in the pedestal, the spectrum is essentially a single spike. The FWHM of the spike is 80 meV in both cases, with ΔE_e=115 meV at 1 nm and ΔE_e=180 meV at 2 nm. It should be noted that the peak photon density with the 100 pC electron beam at 1 nm is only 50% of the value from the corresponding 1 nm simulation of the 300 pC beam, even though it has one third of the charge.

EEHG S2E

The EEHG modulator and chicane specifications used in simulations are listed in Table 2. As with the SXRSS simulations, undulator tapering is also used to optimize performance. Where applicable, benchmarking between Genesis v2 [19], Genesis v4 and with Puffin [20] was performed, with all codes showing similar results. The two 260 nm input lasers are taken to have the same 400 fs FWHM gaussian pulse duration. While this is not essential, with shorter seed lasers it can be difficult to maintain good contrast against SASE from the unseeded portions of the bunch. EEHG simulations were also performed using a variety of lasers and chicane configurations, with similar results.

Recent simulations and analytic studies [14] indicate that moderate initial energy modulations will not affect the EEHG scheme much as long as they do not generate significant current spikes or folding over of the beam phase space. This is because the large initial dispersion in EEHG acts like an effective damping for small modulations with wavelength $\lambda_0 < a\lambda_1/4\pi A_2$, where A_2 is the second energy modulation scaled to the slice energy spread (here $A_2 \approx 6$). In the case of the S2E LCLS-II beams, however, the large tails and strongly chirped regions of phase space combined with the strong first EEHG dispersion lead to significant folding of the the phase space. An example is shown in Figure 5. The result is a beam that is significantly less optimal for clean radiation than the original distribution.

ISBN: 978-3-95450-179-3 doi:10.18429/JACoW-FEL2017-TUB01

Table 2: EEHG Specifications

Element	Strength: 1(2.3) nm	Length
Mod 1	K=25	3.2 m, λ_u=10 cm
	ΔE_1 ≃1(1.5) MeV	
Mod 2	K=12.5	3.2 m, λ_u=40 cm
	ΔE_2 ≃2(3) MeV	
Chic 1	R_{56}=14.4(9.8) mm	9.25 m, L_m=2 m
Chic 2	R_{56}=53(85) μm	2.25 m, L_m=25 cm

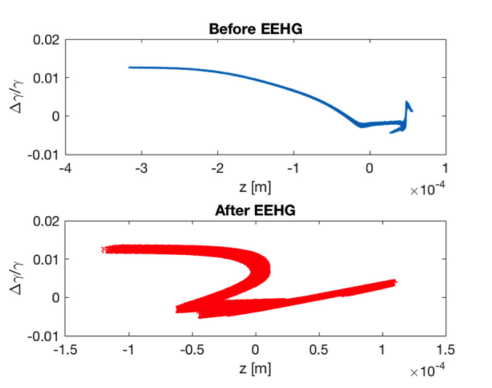

Figure 5: EEHG 300 pC phase space at 1 nm.

The consequences on the FEL spectra are shown in Fig. 6. The full spectral width of the 300 pC beam 2nm spectrum is 2x narrower than the 300 pC SXRSS spectrum due to the smaller pedestal and lack of strong spectral splitting from resistive wakefields. The FWHM of the narrow spike is 60 meV and 45 meV for the 2.3 nm and 1 nm cases, respectively. This is comparable to the 50 meV FWHM with SXRSS, but for EEHG there are 15 times fewer photons within the spike at 1 nm, and 2 times fewer at 2 nm.

The EEHG spectra for the shorter 100 pC beam are also shown in Fig. 6. At 1 nm, the FWHM of the spike is 170 meV, and contains 3e11 photons; a factor of 20 smaller photon

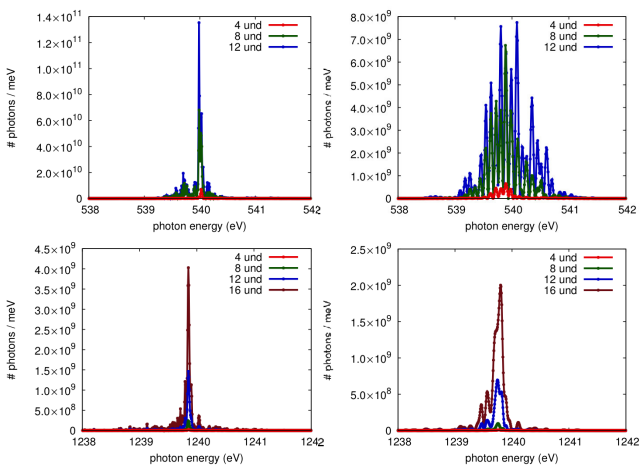

Figure 6: EEHG spectra with 300 pC beam (left) and 100 pC beam (right).

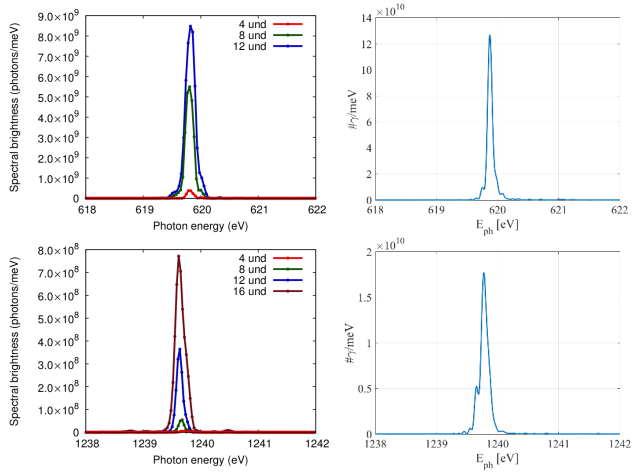

Figure 7: EEHG (left) and SXRSS spectra (right) with ideal 100 pC, 50 fs beam.

density than for SXRSS. At 2.3 nm, the EEHG spectrum has multiple spikes that together cover 500 meV. These are the result of interference between the head and tail current spikes in the e-beam that produce two temporally separated FEL pulses. Such a feature may be useful for phase locked multicolor operations, but this arrangement does not readily produce a single spectral spike.

IDEAL BEAMS

Given the seeding performance of the S2E beams, simulations with ideal, flat-top current profile, 50 fs beams were performed to establish the baseline expectations of EEHG and SXRSS. Beams longer than 50 fs tend to perform worse for both schemes due to the resistive wall wakefields in the LCLS-II undulators, which add nonlinear structure to the otherwise ideal linear e-beam phase space that fragments the spectrum. For beams shorter than 50 fs, the effect of the wake is to introduce a nearly linear chirp in the FEL output.

SXRSS

SXRSS results with an ideal 100 pC beam are shown in Figure 7, seeded from an ideal grating monochromator. The output FEL spectra are single spikes, though the effect of the resistive wall wakefields is revealed in the steady reduction in resolving power from 10k near the grating to around 5k near saturation.

EEHG

The 1 and 2 nm output EEHG spectra are also shown in Figure 7 from two ideal λ_1=260 nm lasers, corresponding to the $a = 130^{th}$ and 260^{th} harmonics. Like the SXRSS spectra, the EEHG spectra are also somewhat broadened by the wakefield-induced chirp, but are still single spike. The EEHG spectra are broader, however, due to two effects. First, there is a harmonic compression effect that shortens the pulse length. Second, the initially flat current profile transforms into a trapezoidal profile after the large chicane.

ISBN: 978-3-95450-179-3 doi:10.18429/JACoW-FEL2017-TUB01

As such, the current at the head and the tail is reduced leaving only a shortened region to lase. Fewer of the total electrons thus participate, so the output power is also less than for SXRSS.

Issues for LCLS-II SXRSS

- Spectral Purity: The SXRSS spectrum is susceptible to pedestal formation and spectral splitting due to long wavelength electron beam phase space modulations, particularly in the longer 300 pC beams.
- Mechanical Inflexibilities and Optical Coupling: In contrast to the existing LCLS SXRSS system, an optimized LCLS-II SXRSS design will include extra mechanical flexibility including rotatable and movable mirrors to better optimize the e-beam/seed beam overlap over 1-4 nm range.
- Heating of compact optical elements: The footprint of the SASE beam on the VLS grating is a few millimeters, and requires cooling of the grating and focusing mirrors to handle the high average power x-ray load (some tens of Watts). Preliminary analysis assuming steady-state conditions indicates that with water cooling, the VLS grating with 5k resolving power would remain within specs for repetition rates up to 100 kHz.

Issues for EEHG

The S2E beams are clearly not well-optimized for external seeding due to the strong non-linear phase space distortions, particularly the large tails. We are currently pursuing beams that can perform much closer to the ideal case. Even so, there are several known issues under consideration for EEHG implementation at soft x-rays:

- Laser Spectral Phase: Spectral phase of the input laser gets multiplied by the large harmonic upconversion factor, but the noise is also filtered by the finite bandwidth of the modulators and FEL. Even orders of spectral phase have the most deleterious effects (ie, linear frequency chirp), but may be mitigated by laser pulse stretching.
- MBI Growth: Strong modulators (K=12-25) increase effect of longitudinal space charge by $1+K^2/2$ factor in drift length. The effect is the worst in 2nd modulator, and can be amplified by chicanes.
- ISR-driven energy spread growth: ISR in second modulator can wash out fine-grained energy structure. This is minimized in current lattice design, but probably precludes slippage-boosted spectral cleaning schemes (ie, harmonic coupling in modulator).
- Large chicane: First chicane (R_{56} ≈15 mm) folds long tails in phase space, and can also generate CSR energy structures that reduce long range coherence of bunching.

Table 3: SXRSS/EEHG Brightness Comparison $B_e[10^{16}]$

Beam	1 nm	2 nm
300 pC	1.0/0.1	5.5/2.6
100 pC	2.4/0.1	3.7/0.2
Ideal	1.1/0.05	7.8/0.8

CONCLUSION

High-resolution numerical simulations with recent S2E 100 & 300 pC beams for LCLS-II indicate that SXRSS delivers pulses with ~ 2 – 20 times higher brightness than EEHG, depending on the tune. This is due to the increased energy spread of the laser modulated EEHG beam and the strong phase space deformation of the non-linear S2E beams in EEHG. SXRSS has the obvious advantage of simplicity of setup, (assuming cooling is adequate), but lacks some of the potential for multipulse and multicolor FEL operations enabled by external seeding. Thus, these seeding options appear to be complementary, given available space in the current LCLS-II beam line design (See Figure 1), as well as expectations with user demand and FEL performance. The performance of these schemes with S2E beams that are better optimized for seeding is currently under study.

REFERENCES

[1] D. Ratner, R. Abela, J. Amann, C. Behrens, D. Bohler, G. Bouchard, C. Bostedt, M. Boyes, K. Chow, D. Cocco, et al., Phys. Rev. Lett. **114**, 054801 (2015a), URL http://link.aps.org/doi/10.1103/PhysRevLett.114.054801.

[2] E. Allaria, D. Castronovo, P. Cinquegrana, P. Craievich, M. Dal Forno, M. Danailov, G. D'Auria, A. Demidovich, G. De Ninno, S. Di Mitri, et al., Nature Photon. **7**, 913 (2013).

[3] G. Stupakov, Phys. Rev. Lett. **102**, 074801 (2009).

[4] D. Xiang and G. Stupakov, Phys. Rev. ST Accel. Beams **12**, 030702 (2009).

[5] D. Xiang, E. Colby, M. Dunning, S. Gilevich, C. Hast, K. Jobe, D. McCormick, J. Nelson, T. O. Raubenheimer, K. Soong, et al., Phys. Rev. Lett. **105**, 114801 (2010).

[6] D. Xiang, E. Colby, M. Dunning, S. Gilevich, C. Hast, K. Jobe, D. McCormick, J. Nelson, T. O. Raubenheimer, K. Soong, et al., Phys. Rev. Lett. **108**, 024802 (2012).

[7] E. Hemsing, M. Dunning, C. Hast, T. O. Raubenheimer, S. Weathersby, and D. Xiang, Phys. Rev. ST Accel. Beams **17**, 070702 (2014), URL http://link.aps.org/doi/10.1103/PhysRevSTAB.17.070702.

[8] Z. T., WangD., C. H., C. H., D. X., D. G., FengC., GuQ., H. M., L. H., et al., Nat Photon **6**, 360 (2012), URL http://dx.doi.org/10.1038/nphoton.2012.105.

[9] E. Hemsing, M. Dunning, B. Garcia, C. Hast, T. Raubenheimer, G. Stupakov, and D. Xiang, Nat Photon **10**, 512 (2016), URL http://dx.doi.org/10.1038/nphoton.2016.101.

[10] Z. Zhao, C. Feng, J. Chen, and Z. Wang, Science Bulletin **61**, 720 (2016), ISSN 2095-9281, URL http://dx.doi.org/10.1007/s11434-016-1060-8.

ISBN: 978-3-95450-179-3 doi:10.18429/JACoW-FEL2017-TUB01

[11] P. Rebernik Ribič, E. Roussel, G. Penn, G. De Ninno, L. Giannessi, G. Penco, and E. Allaria, Photonics **4**, 19 (2017), ISSN 2304-6732.

[12] D. Ratner, C. Behrens, Y. Ding, Z. Huang, A. Marinelli, T. Maxwell, and F. Zhou, Phys. Rev. ST Accel. Beams **18**, 030704 (2015b).

[13] Z. Zhang, R. Lindberg, W. M. Fawley, Z. Huang, J. Krzywinski, A. Lutman, G. Marcus, and A. Marinelli, Phys. Rev. Accel. Beams **19**, 050701 (2016), URL http://link.aps.org/doi/10.1103/PhysRevAccelBeams.19.050701.

[14] E. Hemsing, B. Garcia, Z. Huang, T. Raubenheimer, and D. Xiang, Phys. Rev. Accel. Beams **20**, 060702 (2017), URL https://link.aps.org/doi/10.1103/PhysRevAccelBeams.20.060702.

[15] A. A. Lutman, R. Coffee, Y. Ding, Z. Huang, J. Krzywinski, T. Maxwell, M. Messerschmidt, and H.-D. Nuhn, Phys. Rev. Lett. **110**, 134801 (2013), URL http://link.aps.org/doi/10.1103/PhysRevLett.110.134801.

[16] A. Marinelli, A. A. Lutman, J. Wu, Y. Ding, J. Krzywinski, H.-D. Nuhn, Y. Feng, R. N. Coffee, and C. Pellegrini, Phys. Rev. Lett. **111**, 134801 (2013), URL http://link.aps.org/doi/10.1103/PhysRevLett.111.134801.

[17] A. Marinelli, D. Ratner, A. A. Lutman, J. Turner, J. Welch, F. J. Decker, H. Loos, C. Behrens, S. Gilevich, A. A. Miahnahri, et al., Nature Communications **6**, 6369 EP (2015), URL http://dx.doi.org/10.1038/ncomms7369.

[18] E. Ferrari, C. Spezzani, F. Fortuna, R. Delaunay, F. Vidal, I. Nikolov, P. Cinquegrana, B. Diviacco, D. Gauthier, G. Penco, et al., Nature Communications **7**, 10343 EP (2016), URL http://dx.doi.org/10.1038/ncomms10343.

[19] S. Reiche, Nuclear Instruments and Methods in Physics Research A **429**, 243 (1999).

[20] L. T. Campbell and B. W. J. McNeil, Physics of Plasmas **19**, 093119 (2012), URL http://scitation.aip.org/content/aip/journal/pop/19/9/10.1063/1.4752743.